

PAPER • OPEN ACCESS

## Impact of a strong temperature gradient on grain growth in films

To cite this article: D Zöllner 2022 *Modelling Simul. Mater. Sci. Eng.* **30** 025010

View the [article online](#) for updates and enhancements.

You may also like

- [Phase-field modeling of pores and precipitates in polycrystalline systems](#)  
Julia Kundin, Hassan Sohaib, Raphael Schiedung et al.
- [Molecular dynamics simulations of grain boundary mobility in Al, Cu and -Fe using a symmetrical driving force](#)  
F Ulomek and V Mohles
- [Numerical investigation of the recrystallization kinetics by means of the KWC phase-field model with special order parameters](#)  
Julia Kundin



**IOP | ebooks™**

Bringing together innovative digital publishing with leading authors from the global scientific community.

Start exploring the collection—download the first chapter of every title for free.

# Impact of a strong temperature gradient on grain growth in films

D Zöllner\* 

Graduate Academy, Otto von Guericke University Magdeburg, Universitätsplatz 2,  
39106 Magdeburg, Germany  
B CUBE - Center for Molecular Bioengineering, Technische Universität Dresden,  
Tatzberg 41, 01307 Dresden, Germany

E-mail: [dana.zoellner@ovgu.de](mailto:dana.zoellner@ovgu.de)

Received 4 November 2021, revised 7 December 2021

Accepted for publication 19 December 2021

Published 7 January 2022



CrossMark

## Abstract

The migration of grain boundaries and, therewith, the phenomenon of grain growth depend strongly on the annealing temperature. Generally, higher temperatures are associated with higher mobilities of the boundaries and therewith faster microstructural coarsening. In the present study, the influence of a strong temperature gradient on grain growth in thin films is investigated. To that aim, a modified three-dimensional Potts model algorithm is employed, where the annealing temperature changes with the thickness of the sample taking grain boundary mobility and energy into account. The resulting drag effect has serious consequences for the temporal and spatial evolution of the grain microstructure.

Keywords: grain growth, thin films, temperature gradient, grain boundary mobility, Potts model

(Some figures may appear in colour only in the online journal)

## 1. Introduction

The migration of grain boundaries and, hence, grain growth in polycrystalline solids can be observed among others as a thermally activated process [1–3]. As a result, a polycrystalline grain structure coarsens over time showing a reduction in number of grains per unit volume and associated total grain boundary area. The latter reduces also the total grain boundary

\*Author to whom any correspondence should be addressed.



Original content from this work may be used under the terms of the [Creative Commons Attribution 4.0 licence](https://creativecommons.org/licenses/by/4.0/). Any further distribution of this work must maintain attribution to the author(s) and the title of the work, journal citation and DOI.

energy, whereas a reduced number of grains leads—under the assumption of space filling—to an increase in average grain size. While this general consideration seems relatively simple, grain growth is indeed a complex non-equilibrium process, which can take different shapes. The ideal case or reference case is normal grain growth, where it is assumed, in particular, that all grain boundaries are characterized by the same properties that is by the same grain boundary energy per unit length or area,  $\gamma$ , and same grain boundary mobility,  $m$ . Consequently, the coarsening process is characterized by a unimodal grain size distribution and an average growth law according to which the average grain radius  $\langle R \rangle$  evolves with annealing time  $t$  as [4]

$$\langle R \rangle^2(t) = bt + \langle R \rangle_0^2, \quad (1)$$

where the growth factor  $b$  is a linear function of both, grain boundary mobility  $m$  and grain boundary energy per unit length or area  $\gamma$ . At the same time, the microstructure is in a self-similar state, which can be described among others by a universal and therewith time-independent scaled size distribution  $f(x = R/\langle R \rangle)$ .

Of course, this is a generalization and simplification of the natural process. In reality, the grain boundary properties depend on a number of factors: not only may the crystallographic misorientation play an important role, but also, e.g. segregation at the boundaries [5–7]. Furthermore, it should be noted that the mobility of grain boundaries depends strongly on the annealing temperature,  $T$ , following [8]

$$m = m_0 e^{-\frac{Q^*}{k_B T}}, \quad (2)$$

where  $Q^*$  is the activation energy for grain boundary migration,  $k_B$  is Boltzmann's constant, and  $m_0$  is a quasi-temperature independent pre-exponential factor.

In contrast, a different type of grain growth (to name just one) is called abnormal grain growth, during which some grains show a growth advantage, which allows them to grow to significantly larger scaled grain sizes,  $x$ , than observed for normal grain growth yielding a bimodal size distribution during coarsening [9]. For such a case the average grain size is a very poor descriptor. However, for long annealing times the bimodal distribution may be reduced again to a unimodal shape. While the growth advantage of some grains may be gained by a specific combination of boundary energy and mobility that only few grains in the microstructure possess, grain growth in general is driven by anisotropy of grain boundary energy and mobility [10, 11]. This type of coarsening is particularly complicated to describe analytically.

Independent of the specific type of coarsening, the average grain size increases always over time for each case. This is significant due to the fact that many materials properties such as hardness, strength, and ductility depend strongly on the grain size [12, 13]. Hence, all changes in the microstructure lead to changes of the properties, which may make the material unusable in applications. As a result, understanding grain growth under different conditions is of utmost importance. However, the process of grain growth gets even more complicated when we consider thermal gradients. While, in general, the temperature gradients that occur in most applications are very small making their effects negligible, in certain applications, for example in nuclear reactors, thermal gradients up to  $0.4 \text{ K } \mu\text{m}^{-1}$  can be found [14]. Also, during welding the heat affected zone (HAZ) is characterized by strong spatial temperature gradients that may even change with time [15–17]. Consequently, in such applications, temperature gradients have to be considered as significant driving forces of grain growth.

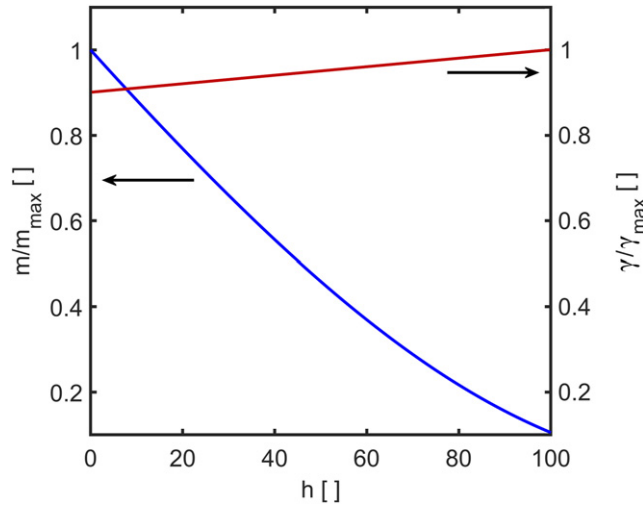


**Figure 1.** Relation between relative mobility and sample thickness according to equation (2) in blue. Variation in grain boundary energy calculated according to [25–27] in red. The size-axis is in arbitrary units, but resembles model units in the simulation model below.  $h = 0$  is the hot surface and  $h = 100$  is the cold surface.

If we consider the simple case of steady-state thermal conduction, then we know that the thermal power,  $\dot{Q}$ , transferred by heat conduction follows Fourier’s law [18, 19]

$$\dot{Q} = -\lambda A \frac{T_2 - T_1}{h} \quad (3)$$

for the simplified case of a solid material with a temperature gradient between two parallel walls. Here  $\lambda$  is the thermal conductivity coefficient, which is, e.g.  $54 \text{ W m}^{-1} \text{ K}^{-1}$  for steel (0.5% C), between  $342$  and  $413 \text{ W m}^{-1} \text{ K}^{-1}$  for copper depending on the temperature, and ranges between  $70$  and  $190 \text{ W m}^{-1} \text{ K}^{-1}$  for aluminum alloys [20]. The areas of the parallel walls are each given by the variable  $A$ , their distance by  $h$ , and their temperatures are  $T_1$  and  $T_2$ , respectively, in equation (3).

Assuming a constant thermal power, the temperature becomes a linear function of the location within the material, from which it results according to equation (2) that  $m \propto e^{-1/T}$ . The resulting relation between mobility and location is shown in figure 1 (blue curve). In order to derive this relation a realistic but non-existing, i.e. non-specific model material was considered. To that aim, an application in a nuclear reactor, where thermal gradients are non-negligible [14], was assumed, where materials such as tungsten are used. In a recent study, Budaev *et al* analyzed mock-ups of ITER tungsten divertor plates using among others electron beam tests with heat loads of up to  $49 \text{ MW m}^{-2}$  [21]. They estimated the penetration depth of temperature during a heat pulse of length  $40 \text{ ms}$  to be approximately  $1.3 \text{ mm}$ . Assuming now for the current investigation a thermal conductivity similar to the one in tungsten as approx.  $140 \text{ W m}^{-1} \text{ K}^{-1}$  and a temperature difference of  $275 \text{ K}$  for  $h = 1 \text{ mm}$  yields a heat flux of  $38.5 \text{ MW m}^{-2}$ , which is realistic.

It should be noted that in figure 1 the above thickness respective location,  $h$ , within the material is transformed already into arbitrary units correlating one-on-one in the simulation below to the units of length as given in terms of Monte Carlo unit (MCU). In particular, the relative mobility is depicted giving the mobility of the boundaries in the material divided by the

corresponding maximum value at the hot surface (blue curve). It can be seen that the boundaries at the hot surface have an advantage of motion compared to the cold surface.

The second temperature dependent factor in equation (1) is the grain boundary energy per unit length,  $\gamma$ , which is part of the growth factor  $b$ . Typically the zero-temperature excess enthalpy is derived by computational studies taking structure and crystallography of the boundary into account. Nevertheless, in practice the finite-temperature grain boundary free energy—the interfacial excess of free energy—is important, but more complicated to calculate.

Already more than two decades ago, Broughton and Gilmer [22, 23] calculated the energy of certain tilt grain boundaries and observed decreases in interfacial free energy with increasing temperature. Also Foiles [24] calculated the interfacial free energy depending on temperature successfully for a  $\Sigma 5$  (310)/[0 0 1] symmetric tilt boundary in Cu. He found that  $\gamma$  decreases indeed by a factor of approximately three when the temperature increases from very low temperatures up to temperatures close to the melting point. In a more recent paper [25], Foiles estimated the temperature dependence of the grain boundary free energy from the temperature dependence of the elastic constants. To that aim, the free energy of the grain boundary as a function of temperature was determined in two manners:

- For temperatures below 25% of melting temperature, the free energy was determined via quasi-harmonic approximation calculations [26].
- For higher temperatures, the free energy was derived via thermodynamic integration using Monte Carlo simulations described comprehensively by Frolov and Mishin [27].

The results show a substantial variation of  $\gamma$  with a clear decrease from zero temperature to temperatures close to the melting point. Of course, any real polycrystalline grain microstructure will have grain boundaries of different type and, therewith a distribution of boundary energies. Exemplarily, Schrott *et al* [28] derived the grain boundary energy landscape using molecular dynamics simulations. However, in order to capture the general effect of the temperature gradient on the coarsening kinetics, in the current work the same general temperature dependence of the boundary energy is assumed as in reference [25]. Furthermore, considering a limited temperature span as in the simulation below, the resulting variation in  $\gamma$  is much smaller compared to Foiles' work [24, 25] as shown in figure 1 (red curve).

Over the years, a number of numerical investigations have been directed towards a better understanding of the general influence of temperature gradients on grain growth, of which selected works are described here shortly:

- Garcia *et al* [29] applied the Monte Carlo Potts model to simulate three-dimensional grain growth with non-uniform grain boundary mobility. They found that grain growth followed locally normal coarsening kinetics in systems with smoothly varying grain boundary mobility. In contrast, whenever the grain boundary mobility had large discontinuities, the growth kinetics was no longer locally normal near the discontinuity.
- Tonks *et al* [30] used a phase field model to investigate the impact of temperature gradients on isotropic grain growth in two dimensions. They observed that the temperature gradient caused significant local migration of the individual grains resulting in larger grains in the hot portion of the polycrystal.
- Tan *et al* [31] used also a Monte Carlo simulation to model grain growth including a spatial temperature profile that varied, however, with time. In addition to two-dimensional verifications and comparisons, they tested their model for a three-dimensional case in the HAZ of a weld.

While these and further works broadened our understanding of grain growth under thermal gradients strongly, there are still a number of questions that remain unanswered.

In the present investigation we analyze the impact of a strong thermal gradient on grain growth in films. To that aim, a three-dimensional sample is modeled taking not only a spatial distribution of temperature and therewith grain boundary mobility and energy into account, but also the influence of the free surfaces. Coarsening kinetics as well as the topology of the resulting microstructure is studied in detail depending on their spatial locations.

## 2. Method

Nearly 40 years ago, the first computer algorithms were developed that enabled researchers to simulate recrystallization, grain growth, and related phenomena in polycrystalline materials. In order to explore different applications, several types of simulations were produced on different size as well as time scales ranging from atomistic simulations to mesoscopic ones. The latter type works, in particular, well on the microstructural level and permits a very selective tailoring of materials parameters. Such simulations enable analyses of large grain structures over long time spans and facilitate comparisons with experiments. As a consequence, for mesoscopic size scales different models were developed over the years, such as the Monte Carlo Potts model, surface evolver, phase-field method, and vertex method (cf, [32–36]).

Among those methods the Monte Carlo Potts model is known for its comparative simplicity in the algorithm. Nevertheless, it can be modified to tailor and model complex problems such as the influence of texture on grain growth [37] or recrystallization and grain growth in specific materials such as aluminum alloys [38].

Specifically, in the Potts model sharp grain boundaries with zero width are assumed. Typically, only two materials parameters characterize the grain boundaries as they have also been mentioned above: the boundary mobility,  $m$ , and energy per unit length or area,  $\gamma$ . Generally, both parameters depend on the misorientation between two adjacent grains [39], but, also on the annealing temperature as discussed above. Moreover, the Potts model requires a given initial microstructure, which is usually defined by a spatial grain distribution of a specific number of grains, including their size distribution, topology, and grain orientation. This microstructure is then projected onto a lattice with  $N$  lattice points, each called a MCU. In the current investigation a three-dimensional square lattice is used. For any given point within the lattice 27 nearest neighbors (nn) are considered for local interactions. For the edges of the lattice specific application-dependent boundary conditions are considered, that is, in the present case, periodic boundary conditions parallel to the temperature gradient and free boundary conditions at the top and bottom surface (perpendicular to the temperature gradient), each having a constant temperature, are implemented.

The smallest time unit of the model (one Monte Carlo step) consists of  $N$  reorientation attempts, where each reorientation attempt itself consist of the following routine:

- (a) For a randomly picked lattice point a new state is generated by changing its orientation to the orientation of one of its neighboring points. Thus nucleation of new (local or global) orientations is prohibited.
- (b) The energy of both, the old and the new state is calculated by the Hamiltonian

$$H = \frac{1}{2} \sum_{i=1}^N \sum_{j=1}^{\text{nn}} \frac{\gamma}{\gamma_{\max}} (1 - \delta(Q_i, Q_j)), \quad (4)$$

where the interaction of the  $i$ th lattice point with all its neighbors is measured by the specific grain boundary energy per unit area  $\gamma$ . For identical neighboring orientations  $Q_i$

and  $Q_j$  the Kronecker delta function is equal to one, and zero for different neighboring orientations. Therefore, naturally only different orientations provide a contribution.

(c) The final orientation of the selected lattice point is determined by a probability of

$$p = \frac{m}{m_{\max}} \frac{\gamma}{\gamma_{\max}} e^{\frac{-\Delta E}{k_B T'}}, \quad \text{if } \Delta E > 0 \quad (5a)$$

and

$$p = \frac{m}{m_{\max}} \frac{\gamma}{\gamma_{\max}}, \quad \text{if } \Delta E \leq 0, \quad (5b)$$

where  $m$  is the previously stated grain boundary mobility. The simulation thermal energy (so-called simulation temperature) is expressed through  $k_B T'$ , which has to be selected with care such that unphysical lattice effects are prevented. Details can be found in reference [40]. This simulation temperature does not relate to the real annealing temperature  $T$  in the experiment. The latter influences solely the boundary mobility and energy.

The maximum values of specific grain boundary energy and mobility are given in equation (5) by the constants  $\gamma_{\max}$  and  $m_{\max}$ , respectively. Assuming normal grain growth (where merely high angle grain boundaries with identical properties contribute to coarsening), leads to the simplification  $m = m_{\max}$  and  $\gamma = \gamma_{\max}$ . While in general grain boundary end energy per unit length are functions of the crystallographic misorientation taking differences in low angle boundaries, high angle boundaries as well as twin boundaries into account, in this present case of isotropic grain boundary energies and mobilities, the above mentioned orientations of grains simply denote the grain numbers. Using this simplification enables us to focus solely on the effect of the temperature gradient without having underlying effects of texture.

The present investigation tackles the problem of a strong temperature gradient on grain growth. To that aim, the dependence of the grain boundary mobility as used in equation (5) on temperature according to equation (2) is taken into account as well as the influence of the temperature on the grain boundary energy as discussed above. In addition, following equation (3) it is assumed that the temperature is a linear function of the location in the material resp. a function of the materials thickness assuming steady-state thermal conduction. The resulting dependencies are shown in figure 1, where the sizes are in arbitrary units, but are associated here with the size unit of the simulation, MCU. In particular, the relations  $\frac{m}{m_{\max}}$  and  $\frac{\gamma}{\gamma_{\max}}$  are given as needed in the simulation algorithm.

The size of the sample is selected as  $500 \times 500 \times 100$  MCU<sup>3</sup> with initially 25 000 grains following a normal size distribution. Initially, the grain sizes are small compared to the thickness of the sample. Then again, the thickness is with 100 MCU large enough such that during coarsening the grains remain relatively equiaxed in contrast to 3D thin film grain growth as described in [41–43] for normal, texture-controlled and triple junction-controlled grain growth, where columnar grains evolve. The annealing temperature is set to its maximum of 300°C resp. 573.15 K at  $h = 0$  MCU and decreases down to 25°C resp. 298.15 K at  $h = 100$  MCU. Hence, the relative mobility  $\frac{m}{m_{\max}}$  starts at  $h = 0$  MCU with a value of one and decreases according to figure 1, whereas the relative energy  $\frac{\gamma}{\gamma_{\max}}$  increases slightly due to the decrease in temperature. The simulation temperature has been selected as  $k_B T' = 0.9$  J according to [40].

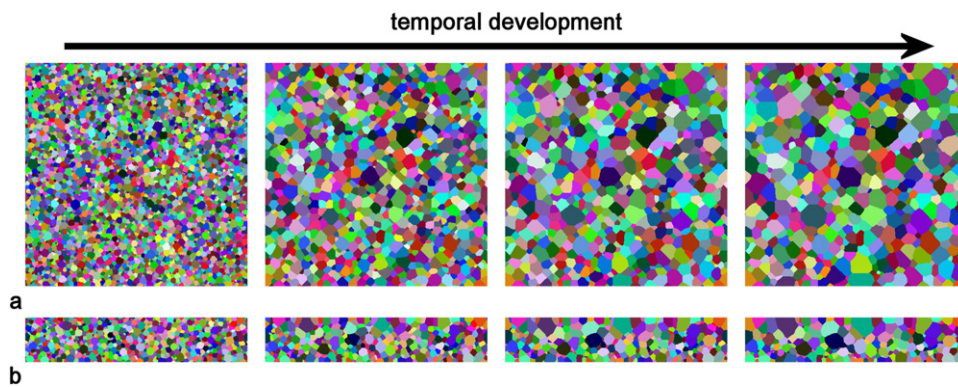


**Figure 2.** Temporal development of the polycrystalline grain microstructure: (a) top view onto the hot surface; (b) side view. The four microstructures are taken at  $t = 0$ ,  $t = 500$ ,  $t = 1000$ , and  $t = 1500$ .

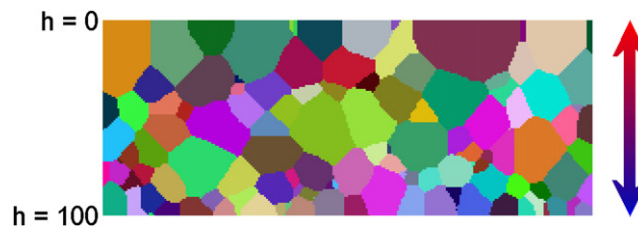


**Figure 3.** Magnified cut-out taken from side view of the simulated sample at the end of the simulation. The arrow marks the temperature profile.

### 3. Results and discussion

After starting the simulation as described above, figure 2(a) shows the temporal development of the top surface of the sample, equivalent to  $h = 0$  MCU in figure 1, which is the hot surface. The coarsening of the polycrystalline microstructure is clearly visible, and the grain microstructure remains uniformly distributed and the grains equiaxed. In contrast, figure 2(b) shows a side view, which is a plane that is parallel to the temperature gradient. The top corresponds again to  $h = 0$  MCU and the bottoms of the images correspond to  $h = 100$  MCU—the cold surface. It can be seen that the microstructure transforms from initially equiaxed grains that are also distributed uniformly in space to showing a significant gradient with larger grains close to the hot surface and small grains at the cold surface, where the coarsening is retarded. This can be seen even better in figure 3, where a cut-out taken from the side view of the simulated sample for long annealing times ( $t = 1500$ ) is magnified. In addition to the spatial changes in grain size, the surface grains at top and bottom align their boundaries perpendicular to the respective surfaces.

In order to take the spatial inhomogeneity in sizes into account, in the following, the evolving microstructure will be analyzed in sections perpendicular to the temperature gradient.

According to equation (1), the average linear grain size in terms of the grain radius evolves as a square-root function of annealing time. Hence, assuming a constant second moment of the scaled grain size,  $\langle x^2 \rangle$ , for self-similar grain growth the average grain area,  $\langle A \rangle = \pi \langle x^2 \rangle \langle R^2 \rangle$ ,

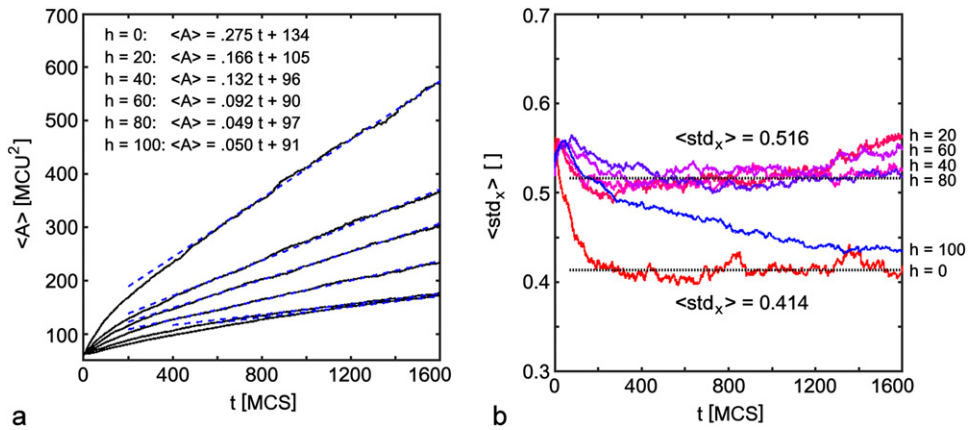


**Figure 4.** Temporal development of: (a) average grain area; (b) associated standard deviation of the scaled grain size, both for six different sections. In figure 4(b), the locations of the sections are given on the right-hand side and the curves are colored accordingly, where blue describes the cold surface and red the hot surface.

increases as a linear function of time. This basic relation  $\langle A \rangle \propto t$  for normal grain growth is shown to be true indeed in figure 4(a) for the different sections from the hot surface at  $h = 0$ , which has the largest slope showing the strongest coarsening, via all inside sections, where the slope gets smaller and smaller with decreasing temperature, to the cold surface at  $h = 100$ , which shows the slowest coarsening. For all sections there are very distinct initial growth regimes with deviating behavior. They indicate that the initial microstructures are far from the later self-similar regimes, which are characterized not only by the linear increase in average grain area but also by constant second moments of the scaled grain size and therewith constant standard deviations  $\text{std}_{x=R/\langle R \rangle}$ . The latter is shown in figure 4(b), where the locations of the sections are given on the right-hand side and the curves are colored accordingly from blue describing the cold surface to red describing the hot surface. It is evident that the sections from within the sample show after the initial period of growth a rather strong fluctuating behavior around the same value of approx.  $\text{std}_x = 0.516$  (dark gray dotted line). This more or less constant value for long annealing times indicates the existence of the above mentioned self-similar state, even though the speed of coarsening is temperature-dependent. Since  $\text{std}_{x=R/\langle R \rangle}$  is very similar for the different sections, the associated scaled size distributions will probably also be very similar comparing different annealing times and different sections. While only four inner sections are shown, a similar behavior can be observed for all sections between approximately  $h \approx 10$  and  $h \approx 90$ . Hence, within the film grain growth follows indeed locally normal coarsening kinetics as predicted in [29].

In contrast, there is a definitive surface effect such that the curves for the surfaces show a deviating behavior. The data for  $h < 10$  and  $h > 90$  approach quickly the curves observed for the limiting cases  $h = 0$  and  $h = 100$ , respectively. In particular, the hot surface at  $h = 0$  reaches after the initial period of time a self-similar state at a much lower standard deviation, whereas the cold surface at  $h = 100$  is characterized by a seemingly extended transition that tends slowly towards the same self-similar state as the hot surface at a lower value of  $\text{std}_{x=R/\langle R \rangle}$  of approx. 0.414. The fact that the cold surface does not show a clear regime with a constant standard deviation within the observed time range corresponds to the fact that the average grain area shows also a slight non-linearity in figure 4(a) (lowest curve).

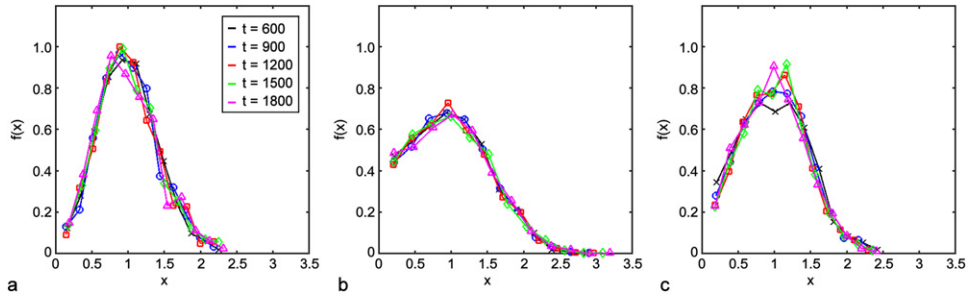


**Figure 5.** Scaled grain size distributions from a large variety of different annealing times ( $t = 600, 900, 1200, 1500, 1800$ ) for: (a)  $h = 0$  (hot surface); (b)  $h = 50$  (middle section), (c)  $h = 100$  (cold surface).

Here it should be noted that in the current investigation the microstructure analyzed perpendicular to the temperature gradient in the thin film is still of three-dimensional characteristics throughout the observed time frame. This is visibly different compared to long annealing times as observed in references [41–43]. In those previous investigations only the first growth regimes were characterized by mostly three-dimensional grain structures just as witnessed here, whereas for long annealing times second growth regimes with columnar grain structures evolved that were coupled to slower coarsening and therewith changes in the average growth law.

A constant standard deviation as (mostly) visible in figure 4(b) after the initial periods of time is a very good indicator of statistical self-similarity, which can be verified by plotting the scaled size distributions. In general, the grain size distribution can be written in its scaling form

$$F(R, t) = g(t) \cdot f(x), \quad (6)$$

where  $g(t)$  is a purely temporal function and  $f(x)$  is a function solely of the scaled grain size  $x = R/\langle R \rangle$ . As a result, for normal grain growth  $f(x)$  is time-independent, for which, therefore,  $\text{std}_x$  is constant as (mostly) observed above. For the present study, the resulting distributions are presented in figure 5 for the hot surface (figure 5(a)), the middle section with  $h = 50$  (figure 5(b)), and the cold surface (figure 5(c)), each for five different annealing times taken from the self-similar regime according to figure 4(b) with  $t \geq 600$ , even for the cold surface, where it is not fully self-similar.

Firstly, at the hot surface (figure 5(a)), the distribution is fairly narrow and close to distributions observed under normal grain growth simulations [44]. It is interesting to note that the distribution is closer to previously observed 3D size distributions of normal grain growth than distributions from 2D simulations even though in the current case a two-dimensional analysis is performed. In addition, it should be noted that despite the fact that the current size distribution is measured at the surface of the sample, the result is remarkably different compared to sections through 3D samples as, e.g. in [45]. The difference originates in the fact that the surface is treated in the current simulation indeed as a surface, whereas in case of figure 3 in reference [45] actual sections through 3D samples were taken. Hence, at the hot surface we can observe a relatively unimpeded motion of the boundaries (having the highest mobility in the sample) resulting in self-similar distributions close to those of normal grain growth.

Secondly, at the cold surface, the distributions as shown in figure 5(c) are slightly broader and characterized by a somewhat larger number of relative small grains. The distributions show a slight temporal development (compare, in particular, curves with black crosses for  $t = 600$

and red squares for  $t = 1200$ ), which is in agreement with the slight temporal change of the standard deviation in figure 4(b) (blue curve,  $h = 100$ ). Hence, over time the distribution will become narrower and will take the shape as in figure 5(a) for the hot surface for very long annealing times. The slightly larger value of  $\text{std}_x$  and therewith the larger broadness of the distribution compared to the hot surface can be a result of the extremely low boundary mobility and the resulting drag effect of the warmer boundaries in the vicinity that move faster.

Thirdly, figure 5(b) shows the scaled grain size distributions for the middle section ( $h = 50$ ). These distributions are significantly broader and show a substantial number of grains with small relative grain sizes as well as grains with sizes up to approximately three times the average value. This spread in size can be assumed to be partly a result of the different drag effects, where the warmer boundaries in the vicinity of the section move faster, while the colder boundaries move slower. However, compared to figures 5(a) and (c), here we are talking about real sections through a 3D sample, for which different distributions are expected anyways [45].

It is of peculiar interest that the distinct shapes of the distributions in figure 5 have been observed previously for totally different types of grain growth, namely triple junction controlled growth and normal grain growth in two and three dimensions, respectively, compare [46–49]. In particular, for grain growth under triple junction control a drag effect of the low junction mobility has been observed to yield such skewed size distributions as in figure 5(b). This is very interesting since, on one hand, in the present case surfaces and sections are analyzed in contrast to the 2D or 3D data in references [46–49] and, on the other hand, the driving forces are significantly different: junction drag in [46–49] versus the strong temperature gradient in the current investigation, which results, however, also in a drag of the faster moving boundaries in the warmer regions of the sample on the slower moving ones in the colder regions.

Beyond the time-independence of the scaled grain size distributions, also topological correlations show a self-similar behavior of the obtained grain microstructures. In particular, the relationship between number of edges,  $n$ , and scaled grain size,  $x$ , is given in figure 6, where the planes (section and surfaces) represented in the three different figures correspond to those in figure 5. In each figure, the data of three different annealing times from the regime with  $t > 600$  (represented by crosses of different colors) fall on top of one another, which is a further indicator for self-similarity. The different widths in the data sets between figures 5(a)–(c) correspond to different broadness of the topological correlations. In order to describe the data set better, each set is averaged into size classes represented in each image by different symbols. Apart from smaller fluctuations, which are due to a limited number of data points falling in the respective binned size class (particularly for large grains as in figure 6(b)), the averaged data can be described well by least-squares fits.

It is very interesting to note that the hot as well as cold surface are both characterized by a quadratic function  $n(x)$ , whereas the inner sections are well-described by linear least-squares fits. While the differences may be explainable already by the different natures of the sections (surfaces versus inner section), in a recent publication [50] the evolution of the topology of the grain microstructure in thin films has been analyzed in detail under normal grain growth conditions. It was observed that even at the surfaces the relation  $n(x)$  of the microstructure can be characterized initially best by a linear least-squares fit within the first growth regime. When the microstructure changes from bulk-like to columnar, not only the speed of growth is reduced but also  $n(x)$  changes to a quadratic relation, which could also contribute to the present observations.

These two different types of functions (linear and quadratic) used for describing the topology agree furthermore with the corresponding scaled grain size: basically, as mentioned above,

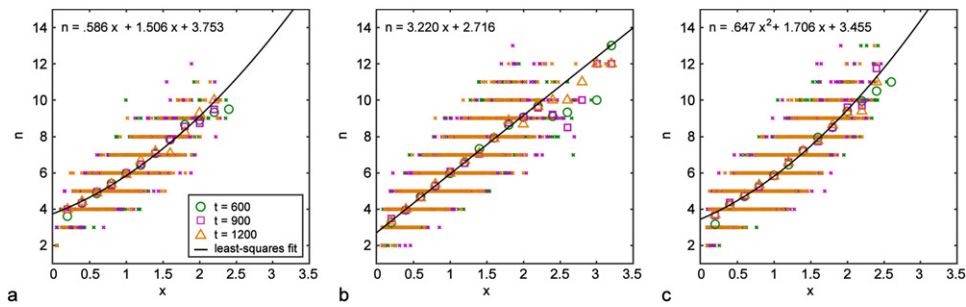


**Figure 6.** Number of edges as function of scaled grain size at three different annealing times for: (a)  $h = 0$  (hot surface); (b)  $h = 50$  (middle section), (c)  $h = 100$  (cold surface). The crosses represent all grains (color coded according to annealing time), whereas the other symbols represent associated data averages.

the scaled size distribution for the hot surface (figure 5(a)) is similar to those observed for normal grain growth, for which a quadratic relation between number of edges and scaled size has been observed previously [49] and is also found in the current investigation (figure 6(a)). In contrast, the scaled size distribution of the inner sections show a distinct distribution (figure 5(b)) similar to those observed under triple junction controlled growth [49], which is associated with a linear relation  $n(x)$  as it is also observed here (figure 6(b)). However, regarding this direct comparison there is a discrepancy: while the scaled size distribution and topology in terms of  $n(x)$  show distinct shapes as observed for either normal or triple junction controlled growth, the average growth law is solely a linear function of annealing time, which agrees only with normal grain growth.

All in all, the author would like to point out that it is not(!) possible to compare the two different behaviors as observed previously (normal grain growth vs triple junction control) and observed here (temperature influence) one-on-one! For normal and triple junction controlled grain growth usually purely two- and three-dimensional investigations were performed. However, in a recent publication [43] grain growth under triple junction control has been investigated in a three-dimensional thin film. It was observed, in particular, that a reduced triple junction mobility yields for a surface analysis not only a quadratic relation between average grain area and annealing time for small grain sizes, but also a skewed scaled size distribution just as observed for 2D and 3D junction control. In contrast, in the current case, where also surfaces have been introduced—just as in [43], different boundary conditions compared to common two- or three-dimensional considerations are observed. Nevertheless, in all of these investigations certain drag effects can be observed either due to a limited mobility of the triple junctions or as in the present case as a drag due to a temperature gradient effecting the growth kinetics.

These differences in  $n(x)$  between surfaces and inner sections indicate possible variations in the morphology of the grains. For an additional analysis the Aboav–Weaire-law [51–54] can be used. Originally, Aboav analyzed already more than 50 years ago how grains in a typical polycrystal are arranged in space finding that they are indeed not disposed randomly, but in a certain order. This enabled him to describe the relation between number of edges  $n$  of a grain and average number of edges of all neighboring grains  $\bar{n}$  of a section through polycrystalline magnesium oxide [51] by

$$\bar{n}n = 5n + 8. \quad (7a)$$

Based on the idea that an infinite 2D polyhedral network, where solely three-fold vertices can be observed, has an average number of edges of all polyhedral cells,  $\langle n \rangle$ , equal to six, Weaire extended equation (7a) taking the second moment of the neighbor distribution,  $\mu_2$ , into account [52]

$$\bar{n}n = 5n + (6 + \mu_2). \quad (7b)$$

This extension inspired above together with further observations of soap foam in a planar section to introduce the geometrical constant  $\alpha$  that depends on the type of cellular pattern [53]

$$\bar{n}n = (6 - \alpha)n + (6\alpha + \mu_2). \quad (7c)$$

Taking the knowledge of the average number of edges of all grains,  $\langle n \rangle$ , into account yields the today well-known Above–Weaire-law

$$\bar{n}n = (\langle n \rangle - \alpha)n + (\langle n \rangle\alpha + \mu_2). \quad (8)$$

Here, again  $\mu_2$  is the second moment of the neighbor distribution, which is equal to the squared standard deviation and  $\alpha$  a structure-specific parameter. As a result of equations (7) and (8), few-edged cells or grains have the tendency to be surrounded by many-edged cells resp. grains and vice versa.

We find in figure 7 that equation (8) is indeed fulfilled for all planes: on the surfaces as well as within the sample showing again self-similar behavior. However, while the average number of edges of the whole ensemble in all the sections is close to six, the width of the distributions are significantly different: the hot surface at  $h = 0$  has the smallest values of approx.  $\mu_2 = 2.08$  averaged over the microstructures shown in figure 6. The cold surface has somewhat larger values with  $\mu_2 = 2.80$ , which decreases slightly over time in agreement with the slight non-self-similarity as noted before. Finally, the middle section is characterized by  $\mu_2 = 3.80$ —a clearly broader neighbor distribution. This is not unexpected as the average number of edges or triple junctions of any two-dimensional grain microstructure with periodic boundary conditions is equal to six, if the microstructure contains only three-fold vertices. Small deviations are due to the rare existence of, e.g. four-fold vertices. Regarding the widths of the distributions it can already be seen above in figure 6 that inner sections have a larger spread in number of edges compared to the surfaces.

Applying now equation (8) to the unconstrained least-squares fits in figure 7 yields for each section two values for  $\alpha$  from slope and constant term using the knowledge of  $n$  and  $\mu_2$  as it can be derived from the microstructures. For the hot surface,  $\alpha$  follows to 1.05 from slope and constant term, respectively, for the cold surface to 0.84 resp. 0.99 from slope and constant term. The fact that the values obtained for the cold surface are not identical and slightly smaller than one can be attributed again to the slight non-self-similarity as observed for standard deviation and scaled grain sizes above. This is furthermore consistent with the slight non-linearity in figure 7(c). In contrast, the inner section shows again self-similar behavior and results in  $\alpha = 1.03$  and  $\alpha = 0.93$  from first and second term. Most of these values are relatively close to one—a fact that is very interesting to note since the previous comparison of size distributions and topology of the current results with junction controlled grain growth has given a good resemblance above. It has been observed in [54] that  $\alpha$  is close to one for growth under grain boundary control (that is, whenever the average growth law follows a parabolic function

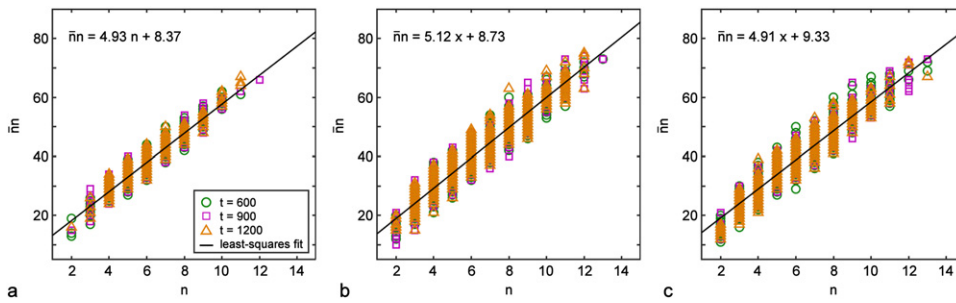


**Figure 7.** Aboav–Weaire-law. Product of mean number of edges of all neighboring grains and number of edges as function of number of edges at three different annealing times for: (a)  $h = 0$  (hot surface); (b)  $h = 50$  (middle section), (c)  $h = 100$  (cold surface). The symbols represent all grains color coded according to annealing time. In addition, linear least-squares fits are given (solid black lines).

of time) as well as under triple junction control (when the average grain size increases as a linear function of time) yielding  $\alpha = 1.0716$  and  $\alpha = 1.0191$ , respectively, in [54]. Hence, the good agreement of the geometrical constant  $\alpha$  for most of the different sections of the current investigation with values as typically observed in normal as well as triple junction controlled grain growth rounds indeed our image off.

It is important to note that in contrast to the relation between number of edges and scaled grain size, the Aboav–Weaire-law, equation (7), has been shown to describe a broad variety of cellular networks, such as nanocrystalline metals, colloidal soap froth structures and even vegetable tissues, e.g. [54–59]. As a result, a variety of structure-specific parameters  $\alpha$  have been observed in the past:

- Stratocumulus clouds show self-organization into honeycomb-like hexagonal patterns, while covering large parts of subtropical oceans. An analysis of these patterns in terms of the Aboav–Weaire-relation yields  $\alpha = 0.93$  for so-called open cells, i.e. cloud-free cells surrounded by cloudy rings, whereas closed cells, i.e. cloudy cells separated by cloud-free rings are characterized by  $\alpha = 0.87$  [56].
- In biomineralized tissues, for sheet nacre morphogenesis [57] an unconstrained linear least-squares fit of equation (8) to the measured data yielded  $\alpha = 1.05$  resp.  $\alpha = 1.10$ .
- Additionally, the prismatic architecture in the specific mollusc shell *Atrina vexillum* shows behavior archetypical for normal grain growth. On top of self-similar scaling, it fulfills also the Aboav–Weaire-law yielding  $\alpha \approx 1.20$  [58], which is clearly larger than expected from 2D normal grain growth simulations.
- For quasi two-dimensional colloidal soap-froth it was found in reference [59] that here also the Aboav–Weaire-law holds yielding a value of  $\alpha = 1.26$ .

Therewith, the current results are fully in the previously observed range.

#### 4. Summary and conclusions

In the present investigation we have analyzed the influence of a very strong thermal gradient on grain growth in thin films. To that aim, a three-dimensional sample has been modeled taking not only a spatial distribution of temperature and therewith a spatial distribution of grain boundary mobility and energy into account, but also the influence of free surfaces. Coarsening kinetics

as well as the topology of the resulting microstructure was studied in detail depending on their spatial locations.

In particular, we find that

- (a) The microstructure evolves from a spatially homogeneously distributed grain structure with equiaxed grains to a very distinct structure showing a spatial gradient with visibly larger grains at the hotter surface compared to the colder surface. The grain boundaries at the surfaces align perpendicular to the surface.
- (b) After an initial period of time that depends on the initial microstructure, the average grain size increases as a linear function of time for all analyzed sections throughout the sample, for which multiple sections have been taken perpendicular to the temperature gradient. The slopes of the linear least-squares fits are a function of the temperature: the higher the temperature the larger the slope. Particularly, at the cold surface a slight non-linearity can be observed, which is a first indicator that a self-similar state has not been reached yet within the observed time frame.

Here it is of great importance to note that in the current investigation the microstructure in the thin film is still of three-dimensional characteristics at the end of the observed time frame. This is visibly different compared to long annealing times as observed in [41–43], where columnar grain structures were found.

- (c) In contrast to the systematic change of the average growth law with annealing temperature, the associated standard deviation (characterizing the size distribution) fluctuates around a constant value of  $\text{std}_x = 0.52$  for long annealing times for all sections within the sample. This indicates the existence of a unique self-similar state for the sections between approximately  $h \approx 10$  and  $h \approx 90$ , where also the size distributions are indeed similar between the different sections and do not change with time. However, the surfaces show clearly smaller values for  $\text{std}_x$ . The associated size distributions are, hence, narrower. In particular, the development of  $\text{std}_x(t)$  suggests that the cold surface has definitively not reached a fully self-similar state.
- (d) It is very intriguing to note that the scaled (self-similar) size distributions are characterized by very distinct shapes. The distributions at the hot surface are similar to those observed for normal grain growth in two or three dimensions. In contrast, the inner sections were expected to show different size distributions, due to the sectioning problem [45]. They show a strong skewness of the time-independent distributions resembling also distributions obtained by triple junction controlled grain growth.
- (e) In addition, the differences in the scaled size distributions are accompanied by differences in the topology of the microstructures: the hot surface with the narrow size distribution is linked to a quadratic relation  $n(x)$  just as observable for normal grain growth, whereas the inner sections with strongly skewed size distributions are linked to linear functions  $n(x)$ .
- (f) Finally, the topology of the microstructures as described by the Above–Weaire-law yields a geometrical constant  $\alpha$  that is typically observed in normal as well as triple junction controlled grain growth for hot surface and inner sections rounding our image off. Only the cold surface yields somewhat lower values. This could also be a result of the non-self-similarity of this specific section as already mentioned under point 3.

These results obtained for a strong thermal gradient can be extrapolated for grain growth under less strong temperature gradients in thin films, for which it is reasonable to assume, in general, a similar behavior. Of course, the film thickness itself and further surface effects may have a likewise important effect, which should be the focus of future studies.

All in all, in a film with a strong temperature gradient the growth of grains at the hot surface with higher mobilities is restricted by the need to maintain contiguity with the smaller grains in the cold, low-mobility region, and vice versa. As a result, a clear three-dimensional microstructural gradient develops.

### Data availability statement

The data that support the findings of this study are available upon reasonable request from the authors.

### CRedit authorship contribution statement

D Zöllner: Conceptualization, Data curation, Formal analysis, Investigation, Methodology, Software, Validation, Visualization, Writing-original draft.

### Conflicts of interest

The authors declare that they have no known competing financial interests or personal relationships that could have appeared to influence the work reported in this paper.

### ORCID iDs

D Zöllner  <https://orcid.org/0000-0002-0413-2700>

### References

- [1] Gottstein G and Shvindlerman L S 2010 *Grain Boundary Migration in Metals* (London: Taylor and Francis)
- [2] Humphreys J, Rohrer G S and Rollett A D 2017 *Recrystallization and Related Annealing Phenomena* (Oxford: Elsevier)
- [3] Gladman T 2004 *Grain Size Control* (Boca Raton, FL: CRC Press)
- [4] Burke J E and Turnbull D 1952 Recrystallization and grain growth *Prog. Metal Phys.* **3** 220
- [5] Rabkin E 2000 *Scr. Mater.* **42** 1199
- [6] Kirchheim R 2002 *Acta Mater.* **50** 413
- [7] Dillon S, Behera S K and Harmer M P 2008 *Acta Mater.* **56** 1374
- [8] Turnbull D 1951 *J. Metals* **3** 661
- [9] Kang S-J L 2005 Abnormal grain growth *Sintering: Densification, Grain Growth, and Microstructure* (Amsterdam: Butterworth-Heinemann) p 117
- [10] Upmanyu M, Hassold G N, Kazaryan A, Holm E A, Wang Y, Patton B and Srolovitz D J 2002 *Interface Sci.* **10** 201
- [11] Hallberg H 2014 *Modelling Simul. Mater. Sci. Eng.* **22** 085005
- [12] Henkel D and Pense A W 2002 *Structure and Properties of Engineering Materials* (New York: McGraw-Hill)
- [13] Callister W D and Rethwisch D G 2014 *Materials Science and Engineering* (New York: Wiley)
- [14] Olander D R 1976 *Fundamental Aspects of Nuclear Reactor Fuel Elements* (Springfield: Technical Information Center, Energy Research and Development Administration)
- [15] Kano S, Oba A, Yang H, Matsukawa Y, Satoh Y, Serizawa H, Sakasegawa H, Tanigawa H and Abe H 2016 *Mech. Eng. Lett.* **2** 15-00481
- [16] Zhang S, Ma Y, Huang S, Youssef S S, Qi M, Wang H, Qiu J, Lei J and Yang R 2019 *J. Mater. Sci. Technol.* **35** 1681

- [17] Mishra S and DebRoy T 2006 *Mater. Sci. Technol.* **22** 253
- [18] Winterbone D E and Turan A 2015 *Advanced Thermodynamics for Engineers* (Amsterdam: Butterworth-Heinemann)
- [19] Sobota T 2014 Fourier's law of heat conduction *Encyclopedia of Thermal Stresses* ed R B Hetnarski (Dordrecht: Springer)
- [20] The Engineering ToolBox 2005 [https://engineeringtoolbox.com/thermal-conductivity-metals-d\\_858.html](https://engineeringtoolbox.com/thermal-conductivity-metals-d_858.html) (accessed 27 December 2021)
- [21] Budaev V P *et al* 2020 *Nucl. Mater. Energy* **25** 100816
- [22] Broughton J Q and Gilmer G H 1987 *J. Phys. Chem.* **91** 6347
- [23] Broughton J Q and Gilmer G H 1998 *Modelling Simul. Mater. Sci. Eng.* **6** 393
- [24] Foiles S M 1994 *Phys. Rev. B* **49** 14930
- [25] Foiles S M 2010 *Scr. Mater.* **62** 231
- [26] Maradudin A A, Montroll G H, Weiss G H and Ipatova I P 1971 *Theory of Lattice Dynamics in the Harmonic Approximation* (New York: Academic Press)
- [27] Frolov T and Mishin Y 2009 *Phys. Rev. B* **79** 045430
- [28] Schratz A A, Steinbach I and Mohles V 2021 *Comput. Mater. Sci.* **193** 110384
- [29] Garcia A, Tikare V and Holm E 2008 *Scr. Mater.* **59** 661
- [30] Tonks M R, Zhang Y, Bai X and Millett P C 2014 *Mater. Res. Lett.* **2** 23
- [31] Tan Y, Maniatty A M, Zheng C and Wen J T 2017 *Modelling Simul. Mater. Sci. Eng.* **25** 065003
- [32] Steinbach I, Pezzolla F, Nestler B, Seeßelberg M, Prieler R, Schmitz G J and Rezende J L L 1996 *Physica D* **94** 135
- [33] Weygand D, Brechet Y, Lepinoux J and Gust W 1999 *Phil. Mag. B* **79** 703
- [34] Barrales Mora L A, Gottstein G and Shvindlerman L S 2008 *Acta Mater.* **56** 5915
- [35] Anderson M P, Srolovitz D J, Grest G S and Sahní P S 1984 *Acta Metall.* **32** 784
- [36] Zöllner D 2016 *Reference Module in Materials Science and Materials Engineering* ed S Hashmi (Oxford: Elsevier) p 1
- [37] Zöllner D and Zlotnikov I 2018 *Comput. Mater. Sci.* **155** 180
- [38] Chekhonin P, Zöllner D, Zimmer E, Scharnweber J, Romberg J and Skrotzki W 2019 *Materialia* **5** 100236
- [39] Ivasishin O M, Shevchenko S V, Vasiliev N L and Semiatin S L 2006 *Mater. Sci. Eng. A* **433** 216
- [40] Zöllner D 2014 *Comput. Mater. Sci.* **86** 99
- [41] Zöllner D 2016 *Comput. Mater. Sci.* **125** 51
- [42] Zöllner D and Zlotnikov I 2019 *Adv. Theory Simulat.* **2** 1900064
- [43] Zöllner D 2021 *Comput. Mater. Sci.* **187** 110104
- [44] Zöllner D and Streitenberger P 2006 *Scr. Mater.* **54** 1697
- [45] Zöllner D and Streitenberger P 2015 *IOP Conf. Ser.: Mater. Sci. Eng.* **82** 012080
- [46] Zöllner D 2012 *Scr. Mater.* **67** 41
- [47] Zöllner D 2011 *Comput. Mater. Sci.* **50** 2712
- [48] Streitenberger P and Zöllner D 2011 *Acta Mater.* **59** 4235
- [49] Zöllner D 2016 *Comput. Mater. Sci.* **118** 325
- [50] Zöllner D 2021 *Comput. Mater. Sci.* **200** 110803
- [51] Aboav D A 1970 *Metallography* **3** 383
- [52] Weaire D 1974 *Metallography* **7** 157
- [53] Aboav D A 1980 *Metallography* **13** 43
- [54] Zöllner D 2013 *Comput. Mater. Sci.* **79** 759
- [55] Mombach J C M, Vasconcellos M A Z and de Almeida R M C 1990 *J. Phys. D: Appl. Phys.* **23** 600
- [56] Glassmeier F and Feingold G 2017 *Proc. Natl Acad. Sci. USA* **114** 10578
- [57] Beliaev M, Zöllner D, Pacureanu A, Zaslansky P, Bertinetti L and Zlotnikov I 2020 *J. Struct. Biol.* **209** 107432
- [58] Zöllner D and Zlotnikov I 2019 *Mater. Horiz.* **6** 751
- [59] Mejía-Rosales S J, Gámez-Corrales R, Ivlev B I and Ruiz-García J 2000 *Physica A* **276** 30